Sensitivity of Reflectance to Water Vapor and Aerosol Optical Thickness

Nitin Bhatia, Valentyn A. Tolpekin, Ils Reusen, Sindy Sterckx, Jan Biesemans, and Alfred Stein

***Abstract*—The atmospheric condition parameters used in the radiative transfer-based atmospheric correction (AC) are often uncertain. This uncertainty propagates to the estimated reflectance. The reflectance, is, however, not equally sensitive to all the parameters. A sensitivity analysis (SA) helps in prioritizing the parameters. The objective of this study was to perform an SA of reflectance to water vapor concentration (wv) and aerosol optical thickness (AOT). SA was performed using the Fourier amplitude sensitivity test (FAST) method, which computes sensitivity indices (SI) of these parameters. Besides variation in the two parameters, we also studied the effect of surface albedo on the SI by quantifying SI for three target surfaces (in the spectral range $0.44-0.96$ μm): 1) a dark target (water); 2) a bright target (bare soil); and 3) a target having low albedo in the visible and high albedo in near-infrared range (forest). For AOT, high (≈ 0.9) SI values were observed at the nonwater absorption wavelengths. For wv, high SI values were observed at wavelengths, where strong absorption features are located and when the surface albedo was high. For the dark target, the effect of AOT was prominent throughout the spectral range. We found that the sensitivity of reflectance to wv and AOT is a function of wavelength, strength of the absorption features, and surface albedo. We conclude that AOT is a more important parameter for dark targets than wv even at the principal absorption feature. For bright targets, the importance of wv and AOT depends on the strength of the absorption feature.**

***Index Terms*—Absorption, aerosol optical thickness (*AOT*), e-FAST, FAST, reflectance, scattering, sensitivity analysis (SA), water vapor.**

I. Introduction

AIRBORNE hyperspectral imaging sensors record radiance, called at-sensor radiance, in narrow contiguous spectral bands as a hypercube. In the absence of the Earth atmosphere, the at-sensor radiance allows to perform spectral analysis of a target surface in the instantaneous field of view (IFOV). In the presence of the Earth atmosphere, however, the spectral analysis is challenging because of scattering and absorption of radiation caused by the atmospheric gases and aerosols. When radiation interacts with an atmospheric particle, electric charges in the particle start oscillating, which causes the electric charges to radiate in all directions [1]. It is this radiation which is called scattered radiation. The scattering reduces the radiant energy of radiation passing through the atmopshere resulting in distorted remote measurement of the surface reflected radiation. Also, due to scattering, the diffuse solar radiation enters into the IFOV of a sensor which is called path radiance. Furthermore, the scattering causes radiation reflected from the background of the target surface to enter into the IFOV of a sensor [2]. In the presence of the atmosphere, at-sensor radiance is, therefore, composed of three radiance components: 1) distorted surface-reflected radiance; 2) path radiance; and 3) background radiance. Another process that distorts the at-sensor radiance is absorption. Like scattering, absorption is a function of wavelength. However, unlike scattering, absorption represents a transformation of the radiation into another form of energy [3]. The spectral ranges at which radiation is absorbed by atmospheric constituents are known as absorption features. Light in a strong absorption feature cannot penetrate the atmosphere, and thus cannot reach to a sensor.

An atmospheric correction (AC) process is used to retrieve surface-reflected radiation from at-sensor radiance. Our focus is on a radiative transfer-based AC. Radiative transfer-based AC, first, simulates transmission of radiation through the atmosphere. These simulations are then used to estimate AC parameters such as path and background radiances. The estimated path and background radiance are used to estimate surface reflectance from the at-sensor radiance [4]. In AC, the transmission simulations are based on a state of the atmosphere represented by the atmospheric condition parameters which define scattering and absorption. Here, the challenge is to know the amount and type of the condition parameters present in the atmosphere at the time of imaging. As these parameters are variable in space and time they can not be measured locally. Thus, in practice, image based methods are often employed to estimate these parameters at pixel level. However, limitations of the image-based methods, such as interpolation and mathematical assumptions, cause uncertainty in the value of the condition parameters. Here, uncertainty refers to dispersion in the values of the condition parameters. Uncertainty in the condition parameters propagates to the estimated target reflectance via the AC.

This study focuses on two atmospheric condition parameters and measures their importance in the AC process. The two condition parameters are: 1) scattering due to aerosols in terms of aerosol optical thickness (AOT) that measures the degree

Manuscript received July 30, 2014; revised March 07, 2015; accepted April 09, 2015. Date of publication May 21, 2015; date of current version July 30, 2015.

N. Bhatia is with Flemish Institute for Technological Research (VITO), Mol 2400, Belgium, and also with ITC, Faculty of Geo-Information Science and Earth Observation, University of Twente, Enschede 7514, The Netherlands (e-mail: nitin.bhatia@vito.be).

V. A. Tolpekin and A. Stein are with ITC, Faculty of Geo-Information Science and Earth Observation of the University of Twente, Enschede 7514, The Netherlands (e-mail: v.a.tolpekin@utwente.nl; a.stein@utwente.nl).

I. Reusen, S. Sterckx, and J. Biesemans are with Flemish Institute for Technological Research (VITO), Mol 2400, Belgium (e-mail: ils.reusen@vito.be; sindy.sterckx@vito.be; jan.biesemans@vito.be).

Digital Object Identifier 10.1109/JSTARS.2015.2425954

to which aerosols impede the transmission of radiation; and 2) absorption due to water vapor. Water vapor is an absorbing gas that effects the transmission of the radiance by absorbing the radiation at water absorption features. Alternatively, values of these condition parameters are estimated by image-based techniques [5], [6]. These techniques often use interpolation and mathematical assumptions to infer pixel-wise values. Therefore, the two condition parameters are uncertain. The uncertainty in AOT and water vapor refers to the degree to which their true value and concentration are known at the time of imaging, respectively.

The objective of this study is to quantify the importance of the absorption effect due to water vapor concentration (wv) and the importance of the scattering effect due to aerosols in terms of AOT in estimating reflectance via the AC.

In the literature, van de Vlag and Stein [7] focused on incorporating uncertainty at various levels of the decision tree for image classification. In [8], the estimation of uncertainties in satellite-derived inherent optical properties was investigated, whereas Beekhuizen *et al*. [9] investigated the propagation of digital elevation model uncertainty to the geometrically corrected product. In [10], the effect of uncertainty propagation from AOT, due to a simplification of azimuth angle, to the surface reflectance was studied. In [11], the dependence of AOT on wavelength was studied. In [12], the retrieval of AOT and its sensitivity to surface albedo were studied. In [13], a sensitivity analysis (SA) was performed using synthetic MERIS data to investigate the impact of atmospheric state, the target elevation or the surface roughness on AOT, and column water vapor. To our knowledge, previous studies did not provide quantitative information on the importance of the condition parameters in the AC.

II. Methods

The importance of the two condition parameters was quantified using an SA. An SA provides information on the contribution of sources of variation to dispersion in the output. An SA is used as well to investigate the importance of parameters to a model [14]. Two types of SA are commonly distinguished: 1) a local and 2) a global SA. A local SA perturbs each parameter with respect to its baseline value. Usually, a local SA is carried out by determining partial derivatives and evaluating them within an interval. The interval is usually small which does not cover a range of uncertainty in a parameter. Thus, this method partially covers parameter uncertainty. Furthermore, a local SA is unfeasible to implement for a processing chain because of complexity of the processing chain—it is unfeasible to compute its partial derivatives. On contrary to a local SA, a global SA perturbs parameters by exploring their probability distributions that cover a whole range of parameter uncertainty. A global SA allows a simultaneous perturbation of the parameters. Besides, a global SA facilitates a vast range of implementation methods and sampling strategies, like Monte Carlo simulation (MCS) and latin-hypercube simulation. Furthermore, a global SA can be implemented without knowing the structure of a model. This makes a global SA more robust and useful for complex modeling. For the AC, we used Central Data Processing Center (CDPC) [15], which is the standard airborne image processing chain at the Flemish Institute for Technological Research (VITO) as a case study. The type, complexity, and structure of the AC model used in the CDPC are as follows. The radiative transfer-based AC first simulates the atmospheric transmission. In the CDPC, the MODerate resolution atmospheric TRANsmission (MODTRAN-4) model is used to simulate the atmospheric transmission. MODTRAN is a complex model with a large number of parameters. Thus, for MODTRAN, factors such as the internal sources of variation, relations between parameters are too complicated to fully explore. Therefore, we consider MODTRAN as a black box model. For such a model, SA methods such as a local SA or a global SA such as [16] and [17] cannot be used because these methods assume that a model structure is known. In [18], ANOVA-based SA techniques were discussed, which assume no model structure; thus, we found them the most suitable for MODTRAN. Two classes of ANOVA-based SA are found in the literature [14]: 1) the Sobol method [19] and 2) the Fourier amplitude sensitivity test (FAST) method [20]. The disadvantage of the Sobol method is its computational inefficiency. It requires a large number of model evaluations, which is a serious concern for the complex MODTRAN model. In contrast, the FAST method is computationally more efficient; it computes the sensitivity index (SI) of parameters to a model as indicators of the parameters importance. Thus, in this research, we used the FAST method to measure the importance of the two condition parameters.

The two condition parameters: 1) water vapor concentration (wv) and 2)AOT, which are derived in the CDPC from image-based methods [5], [6]. In MODTRAN-4, AOT can be set using $visibility$ [21]. Physically, AOT and $visibility$ are not directly related because $visibility$ refers to horizontal distance, surface meteorological range in kilometers, at which an object can be discerned. In MODTRAN, however, $visibility$ specifies the scaling of the aerosol size distribution that directly effects AOT [21], [22]. Therefore, $visibility$ in MODTRAN is used as a parameter to set AOT and we used the term $visibility$ to refer to AOT where appropriate.

As an input to the AC process, we used at-sensor radiance obtained from the airborne hyperspectral HyMap sensor data of the Millingerwaard area in The Netherlands acquired in 2004, shown in Fig. 1 (left). The spatial resolution of the image is $2.5\,\mathrm{m}$ along track and $2.0\,\mathrm{m}$ across track. The 128 spectral bands are divided into four wavelength ranges with each 32 bands ($0.45-0.89$, $0.89-1.35$, $1.4-1.8$, and $1.95-2.48\ \mu\mathrm{m}$). The image-based methods used to estimate the condition parameters use spectral bands in the visible (VIS) and near-infrared (NIR) regions.

A. SA Implementation

The FAST method was originally developed within the MCS framework. Thus, an initial step in the FAST method is to develop a joint distribution of parameters and then sample multiple (m) parameters values from the joint probability distribution. For the m parameters values, m outputs are generated.

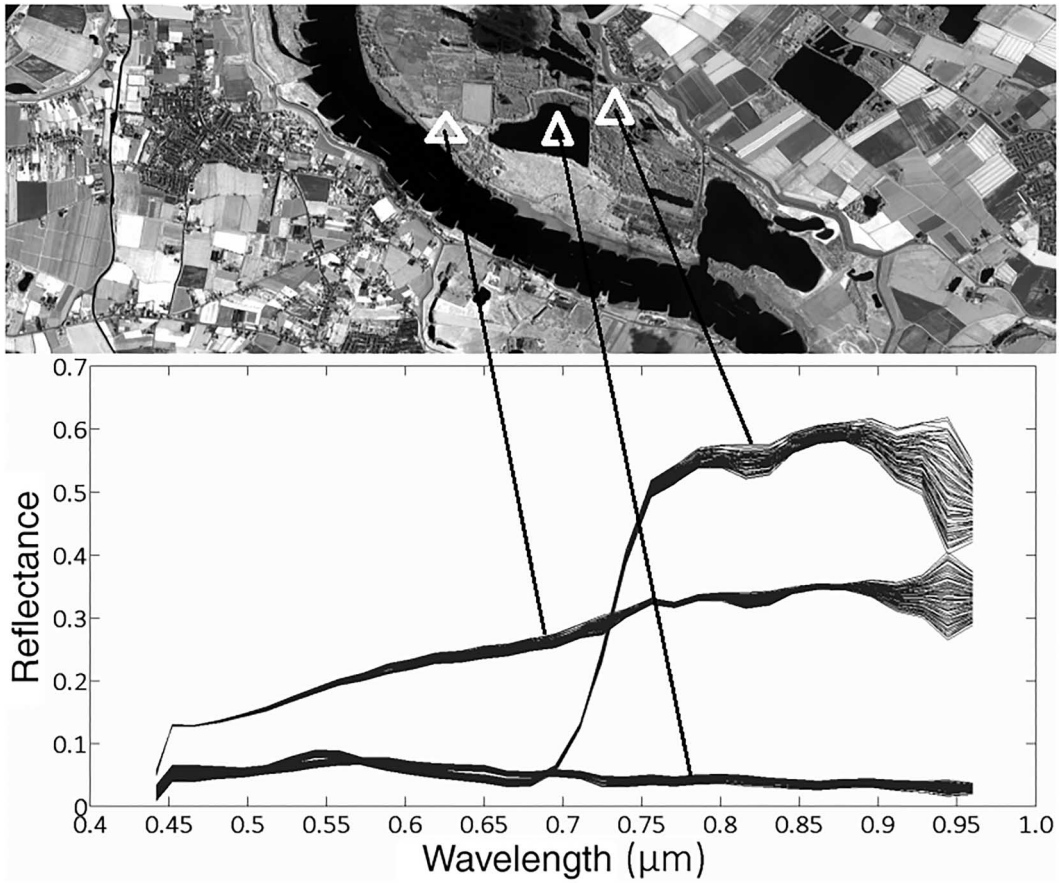

Fig. 1. HyMap sensor image of the Millingerwaard area in the Netherlands acquired in 2004. Three target surfaces (shown with triangle): water (dark target), bare soil (bright target), and forest (dark in visible and bright in the NIR spectral region), were used to study the effect of surface type on the sensitivity index. The mean value, from the 16 pixels (4×4 window), was used for each target surface. The multiple realizations of the spectra were obtained by varying the atmospheric state using wv and AOT in the AC.

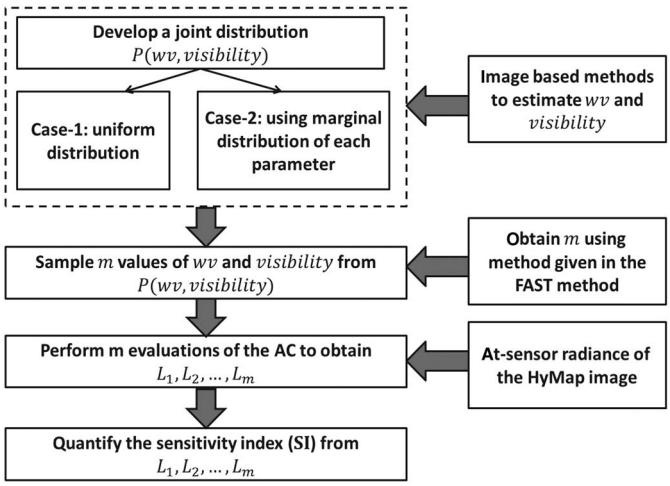

Fig. 2. Process of quantifying the sensitivity indices is depicted in the block diagram.

A Fourier analysis is applied to a set of model output to compute the proportion of the output uncertainty contributed by each parameter. This proportion of uncertainty is defined as the SI. In this study, the simulation of multiple atmospheric transmittances from m samples of wv and $visibility$ were used to estimate m realizations of the target reflectance $(L_1, \ldots, L_m)$. We have summarized the above process in Fig. 2. We are now going to explain the methodology in detail.

Step 1) Develop a joint distribution $P(wv, visibility)$: Here, we studied two test cases that were based on the possibility of two types of joint distribution for the condition parameters. The goal was to study the effect of the joint distribution on the FAST SI. The two cases are as follows:

Case 1. Uniform joint distribution. We obtained ranges of wv and $visibility$ derived from the image-based methods. Using the ranges of the condition parameters, we developed a joint uniform distribution.

Case 2. The probability densities of wv and $visibility$, and their statistical relation were used to derive their joint distribution. We developed marginal distribution of each parameter. Besides the marginal distributions, we also studied the statistical relation between the condition parameters. Aerosols and water vapor interact in the atmosphere. Many studies have explained the effect of water vapor on the size distribution and optical characteristics of the atmospheric aerosols [23], [24]. The variation in

TABLE I
VALUES OF Ω_N AND d_h USED TO CALCULATE FREQUENCIES IN THE FAST METHOD ARE SHOWN FOR $N = 1, 2, 3, 4$

N	Ω_N
1	0
2	3
3	1
4	5

h	d_h
1	4
2	8
3	6
4	10

N refers to an interference factor that determines the number of Fourier coefficients retained in calculating partial variance (SI) due to k_1 and k_2.

wv, thus, affects AOT. Therefore, we considered a statistical relation between these parameters while developing their joint distribution. For this purpose, we analyzed their scatter plot and measured the correlation and the p-values.

Step 2) Sample m values of wv and $visibility$ from $P(wv, visbility)$: For sampling, simultaneous perturbation to the condition parameters is used. This was achieved by using the FAST search curve. The basic idea of the FAST search curve is to transform a n-dimensional parameters space into a one-dimensional (1-D) s space, such that variation in s generates a search curve that traverses $P(wv, visibility)$ and generates multiple wv and $visibility$ samples.

Here, we represent the two condition parameters as (k_l) (with $l = 1$ for wv and $l = 2$ for $visibility$). For the two parameters, the equation of the search curve can be written as

$$k_l = \frac{1}{2} + \frac{1}{\pi} \arcsin(\sin \omega_l s) \tag{1}$$

where ω_l is a frequency assigned to each parameter. The frequencies used in the FAST search curve were obtained as follows [25]:

$$\begin{cases} \omega_l = \Omega_N, & \text{with } N = 4 \text{ for } l = 1 \\ \omega_l = \omega_{l-1} + d_h, & \text{with } h = (n+1) - l \text{ for } l = 2. \end{cases} \tag{2}$$

We used $N = 4$, as recommended by [25] and [26], which is an interference factor that determines the number of Fourier coefficients retained in calculating the partial variance (SI) due to k_1 and k_2. Thus, according to Table I, $\omega_l = 5$ for $l = 1$ and $\omega_l = 9$ for $l = 2$.

The number of samples is a critical parameter in MCS-based SA as it determines the number (m) of times a model is evaluated. The calculation of m in the FAST method is based on the Nyquest criterion and gives the relation between the maximum frequency assigned to parameters and m. Here, for reference, we have included the formula to calculate m [20]

$$m = (2 \cdot N \cdot \omega_{l_{max}}) + 1 \tag{3}$$

with $\omega_{l_{max}}$ the maximum of ω_l. For the FAST method

$$\omega_{l_{max}} = 9; \quad \text{thus, } m = 73.$$

Thus, using the FAST search curve, we obtained 73 samples of the two condition parameters, which we used to propagate the two condition parameters to the reflectance via AC.

Step 3) Perform m evaluations of an AC for m values of wv and $visibility$ to obtain $L_1, \ldots, L_m$: the radiative transfer-based AC process, first, estimates the correction parameters. Then, using the correction parameters, the surface reflectance is estimated. We now explain how MODTRAN is used to estimate the correction parameters. MODTRAN-4 is executed for specified atmospheric state, sun-view geometry, viewing zenith and azimuth angles, and sensor altitude. The MODTRAN-4 output includes the following:

1) A total path radiance (L_{path}) that represents radiance scattered in IFOV of a sensor. The total path radiance; thus, consists of the scattered solar and the background radiation.
2) A total ground radiance (L_{gnd}) that represents radiance reflected by a surface considering that the surface is illuminated by the direct light and the diffused light.

To calculate the correction parameters for a specified atmospheric state, viewing and illumination geometry, it is sufficient to execute three runs of MODTRAN-4. Each run is for a spectrally flat surface albedo of 0.0, 0.5, and 1.0, respectively [27], [28]. The three flat surface albedos (0.0, 0.5, 1.0) indicate: 1) no incident radiation is reflected by the surface; 2) half of the incoming radiation is reflected by the surface; and 3) all of the incoming radiation is reflected by the surface, respectively. The three MODTRAN-4 runs result in three sets, for each flat surface albedo, of the total path radiance ($L_{\text{path0.0}}$, $L_{\text{path0.5}}$, $L_{\text{path1.0}}$), and three sets of the total ground radiance ($L_{\text{gnd0.0}}$, $L_{\text{gnd0.5}}$, and $L_{\text{gnd1.0}}$). From the three sets of the two radiance terms, the correction parameters can be calculated using the relation

$$\begin{aligned} c_1 &= -L_{path0.0} \\ c_2 &= 1.0 + \frac{L_{\text{path0.5}} - L_{\text{path0.0}}}{L_{\text{gnd0.5}}} \\ c_3 &= 1 - c_2 \\ c_5 &= \frac{(2.0 \cdot L_{\text{gnd0.5}}) - L_{\text{gnd1.0}}}{L_{\text{gnd0.5}} - L_{\text{gnd1.0}}} \\ c_4 &= (1.0 - c_5) \cdot (L_{\text{gnd1.0}} + L_{\text{path1.0}} \\ &\quad - L_{\text{path0.0}}) + (c_5 \cdot c_1) \end{aligned} \tag{4}$$

where c_1 is the path radiance; c_2 and c_3 quantify the background effect ($c_2 = 1$ and $c_3 = 0$ means no background effect); c_4 is proportional to the product of transmittance toward the surface and transmittance from surface toward the sensor; and c_5 equals spherical albedo for illumination from below. These correction parameters are constant for a specified atmospheric state, and viewing and illumination geometry; however, the parameters have to be calculated at each wavelength [27]. From the correction parameters, the surface reflectance is estimated using the method described in [4] and presented as follows:

$$L_i = \frac{c_1 + c_2 \cdot L_{\mathrm{sensor}_i} + c_3 \cdot L_{\mathrm{bg}_i}}{c_4 + c_5 \cdot L_{\mathrm{bg}_i}} \tag{5}$$

where L_{sensor_i} is the at-sensor radiance at $i\mathrm{th}$ pixel; L_{bg_i} is the background radiance that can be calculated from the at-sensor radiance. The correction parameters were calculated for m FAST samples that describe different atmospheric states. This resulted in 73 realizations of the estimated reflectance.

To study the effect of the surface albedo and wavelength on the SI, three target surfaces were utilized. The three targets are as follows: 1) a low reflectance, dark target (water); 2) a high reflectance, bright target (bare soil); and 3) a surface with low reflectance in the VIS and high reflectance in the NIR range (forest). The location of the pixels used to represent the three surfaces is depicted in Fig. 1. We used the mean value of pixels in a 4×4 window for each of the target surfaces.

Step 4) Quantify the sensitivity indices of L to variation in wv and $visibility$: The multiple target reflectances were Fourier analyzed using the frequencies (ω_l) assigned to k_l to calculate the Fourier coefficients. From the Fourier coefficients, sensitivity indices of k_l were calculated using the method [20]

$$SI_{\omega_l} = \frac{\sigma_{\omega_l}}{\sigma} \tag{6}$$

where σ is the total variance of the output indicating the dispersion in L due to uncertainty in both the parameters k_1 and k_2, and σ_{ω_l} indicates the partial variance due to parameter k_l. The indices SI_{ω_l} are the first-order sensitivity indices that correspond to the main effect. They represent the contribution of wv and $visibility$ to L.

In this section, we have presented the SA methodology that is based on the FAST method. The FAST method can compute the first-order indices (SI) that correspond to the main effect; however, it cannot compute the total SI (TSI). The TSI is considered as a better measure of sensitivity of a parameter than SI as it also measures the effect of parameters interaction [14]. In [26], the extended FAST (e-FAST) technique that preserves the computational efficiency of the FAST is proposed and can quantify the TSI. Therefore, we also performed the SA using the e-FAST method and quantified the TSI to compare the FAST and e-FAST methods.

III. Results And Discussion

In this section, we present and discuss the results achieved for the two cases.

Step 1) Develop the joint distribution $P(wv, visibility)$: For Case 1, we obtained the ranges of the condition parameters from the image-based methods. For the HyMap image of the study area, in total, 1420 observations of $visibility$ were obtained; however, wv was observed at each pixel (7.87×10^5). The ranges of the two parameters observed were $1.6{-}2.9\,\mathrm{g \cdot cm^{-2}}$ for wv and $20{-}120\,\mathrm{km}$ for $visibility$. The sampling region for Case 1 is the entire range of these parameters.

For Case 2, we first analyzed the scatter plot and measured the correlation coefficient and p-value to investigate a relation between the two parameters. Here, we only used 1420 observations of wv that corresponds to pixels for which $visibility$ was measured. Therefore, the range of wv shown in Fig. 3 is different from the range used in Case 1. The scatter plot in Fig. 3, suggested no direct evidence for any relations between the parameters. From the correlation test, we found a low value (-0.0184) of the correlation between the two parameters. From the p-value test, we obtained $p = 0.5144$. From the scatter plot and the statistical tests, we observed no relation between the parameters.

Because no statistical relation between the condition parameters was found, we focused on marginal distributions of the condition parameters to develop the joint distribution. For this purpose, we first examine the histogram of the two parameters. In Fig. 3, the histograms of the two parameters are shown. The histogram of wv [Fig. 3 (x-axis)] indicates that a normal Gaussian distribution closely represents the marginal distribution of wv. The histogram of $visibility$ [Fig. 3 (y-axis)] suggests that $visibility$ is having a large number of occurrences far from the mean of the distribution. Statistically, this indicates a long-tail distribution. Thus, we used a log-normal distribution to represent the marginal distribution of the $visibility$. In Fig. 3, the sampling region for Case 2 is indicated by the high-density region.

We now discuss the relevance of considering the two cases for this study. Case 1 represents a situation when one does not have information about the probability density or the statistical relation of wv and $visibility$. In this situation, one can assume a uniform distribution in a reasonable range. This range can be presumed on the basis of historic data, expert's opinion on similar areas, weather conditions, etc. Here, we obtained the range of wv and $visibility$ from the image-based methods. Whereas, Case 2 considers a situation in which one has a detailed knowledge about the probability densities and statistical properties of wv and $visibility$.

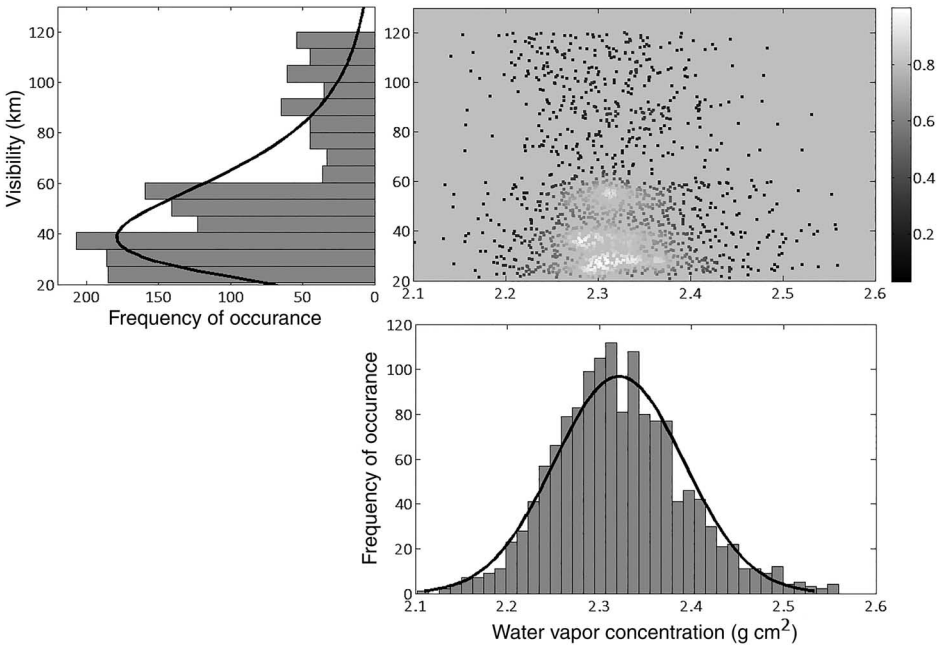

Fig. 3. Plot depicts three informations: scatter plot between estimated $visibility$ and the corresponding wv values; histogram of wv and $visibility$; and the sampling region as indicated by a high-density region.

The knowledge about wv and $visibility$ is used to develop $P(wv, visibility)$. The two cases provide ample opportunity to investigate the significance of probability densities of wv and $visibility$ in quantifying their importance in the AC.

Step 2) Sample m values of wv and $visibility$ from $P(wv, visibility)$: In Fig. 3, the sampling region for Case 2 is indicated by the high-density region. In this step, we discuss the performance of the search curve in terms of how effectively it can sample the sampling region of the joint distribution.

An important characteristic of the search curve is that it perturbs the parametric space simultaneously and passes through each point in the parametric space, such that the path of the search curve corresponds to a joint probability density of parameters [20]. This can be achieved if the frequencies chosen are incommensurate. For implementation point of view, commensurate frequencies (integer frequencies) are used instead of incommensurate frequencies. Due to the use of integer frequencies, two types of errors arise: 1) the search curve is not space filling, which means that it does not pass through each point in $P(wv, visibility)$; and 2) the interference effect—the Fourier coefficients. We, however, observed that the reflectance was not sensitive to small variation in wv and $visibility$. The fact that the search curve is not space filling, therefore, does not effect the SA and the density of points sampled by the search curve is appropriate for the SA. This implies that the use of integer frequencies does not affect the joint probability density of the parameters. The parameter N in (3) is used to avoid the interference of the Fourier coefficients.

In Fig. 4, the scatter plot and the histogram of the sampled values of wv and $visibility$ are for Cases 1 and 2. Comparing the range of the sampled values with the range of the sampling region of $P(wv, visibility)$ indicated with high-density region in Fig. 3, we observed that the sampling is effectively performed from the required region of the joint probability of the two parameters. Also, comparing the histogram of the measured wv and $visibility$ with the histogram of the sampled values of these parameters, we observed that they are similar. This shows that the FAST samples match to the two parameters probability distribution and that the FAST search curve is an effective sampler.

Step 3) Perform 73 evaluations of an AC for wv and $visibility$ to obtain $\mathrm{L}_1, \ldots, \mathrm{L}_\mathrm{m}$.

Step 4) Quantify the sensitivity indices of L to variation in wv and $visibility$: The AC is performed on the HyMap images for the spectral range $0.44-0.96$ μm. The HyMap bands close to the water vapor absorption features are located at 0.58, 0.65, 0.72, 0.82, and 0.94 μm. Equations (4) and (5) express the relation between the atmospheric state, the correction parameters, and the estimated reflectance. The outcome of 73 AC simulations are depicted in Fig. 1 for the three surface albedo. From these results, we observed that the estimated reflectance at 0.94 μm showed largest variations. In the design of our experiments, sources of variation other than wv and AOT were considered as constant; thus, the variation in the reflectance at the principal absorption feature can be attributed to wv and AOT. This variation near the principal water absorption feature (0.94 μm) is often termed as over and

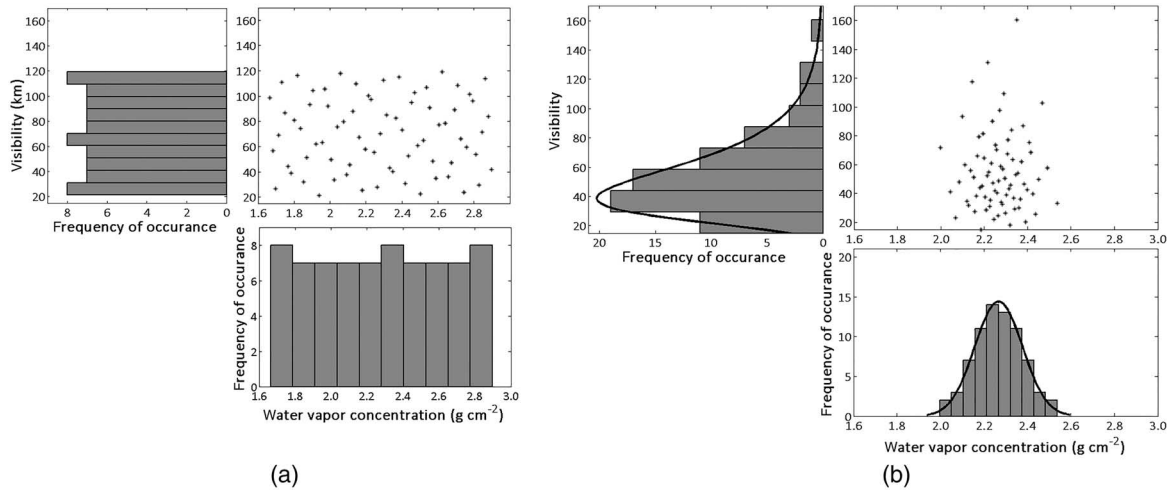

Fig. 4. Samples obtained from the FAST search curve for the two cases. From these samples, we observed that the sampling is effectively performed from the required region as per $P(wv, visibility)$. Also, comparing the histogram of the measured wv and $visibility$ with the histogram of the sampled values, we observed that they are similar. (a) Scatter and histogram plots of FAST samples for Case 1. (b) Scatter and histogram plots of FAST samples for Case 2.

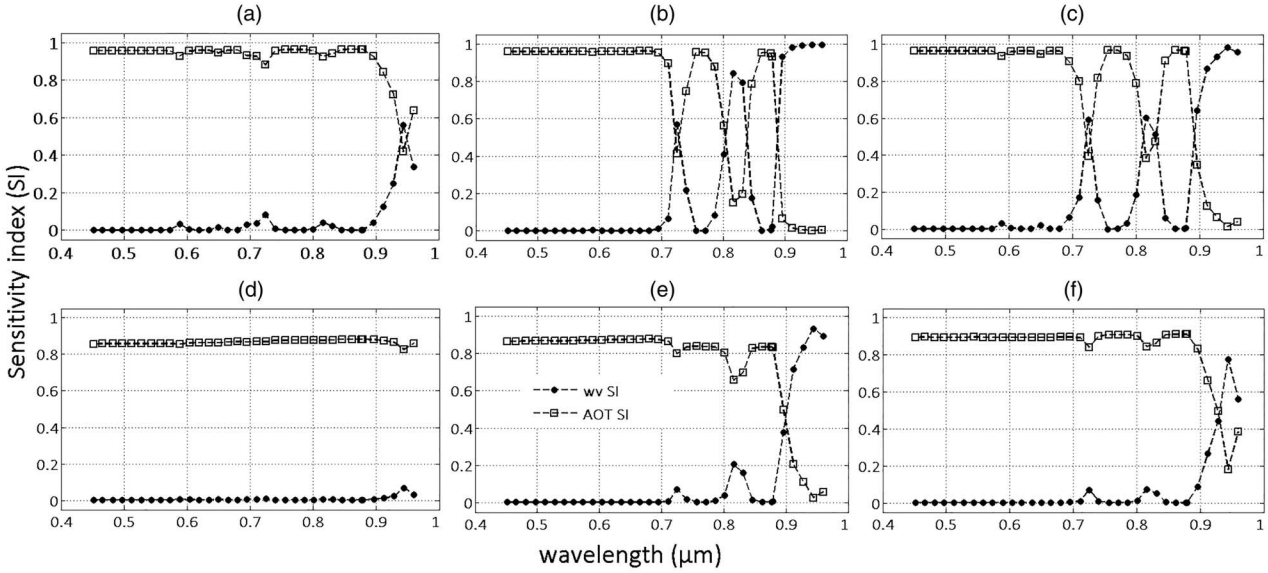

Fig. 5. Sensitivity indices for the three target surface for the two cases. (a)–(c) Depicts results from Case 1 for water, forest, and bare soil targets, respectively. (d)–(f) Illustrate results from Case 2 for water, forest, and bare soil targets, respectively.

under estimation of reflectance. The over and under estimations occur because of uncertainty in wv and AOT. This indicates that the reflectance is sensitive to variations in wv and AOT. These results, however, are only a qualitative indicator of the sensitivity.

We now discuss the results of the importance of the two parameters quantified by their SI presented in Fig. 5. The results in Fig. 5(a)–(c) are results from Case 1. The results in Fig. 5(d)–(f) are results from Case 2. Here, we are discussing the two cases separately.

Case 1. From the indices shown in Fig. 5(a)–(c), we observe that in the spectral range $0.44-0.96$ μm, AOT remains an important parameter, as its sensitivity indices are high (>0.9). The AOT indices, however, vary at the water absorption features (0.58, 0.65, 0.72, 0.82, 0.94 μm). Likewise, indices of wv were high at the absorption features. At the weak absorption features such as at 0.58 and 0.65 μm, the AOT indices only slightly decreased, whereas the wv indices showed very small increase. From these results, we concluded that the influence of AOT in the spectral range $0.44 - 0.96$ μm also depends on the strength of the absorption feature. This implies that in the nonabsorbing wavelengths and at the weak absorption features, the AOT plays an important role, which can be observed from high SI values for AOT in these wavelengths. Likewise, for

strong absorption features, the importance of wv was larger than the scattering effect, resulting in low indices for the AOT.

Besides the strength of the absorption features, another important factor that affects the sensitivity of the two parameters is the surface albedo. From Fig. 5(a)–(c), we observed that for the low albedo target, the effect of scattering was more prominent in the entire spectral range. Even at the principal absorption feature (0.94 μm), the sensitivity indices for AOT and wv are almost equal. The difference in sensitivity indices over bright and dark targets is primarily due to the difference in radiation energy reflected by the bright and the dark targets. The bright target reflects more radiation energy than the dark target. Thus, for the bright target, the majority of the at-sensor radiance consists of photons that are not scattered. In contrast, above the dark target, most of the photons are scattered, which results in strong sensitivity to AOT [29]. For the bare soil and the forest pixels which are bright (reflectance in the range of 0.4–0.7) at 0.94 μm, the wv sensitivity indices were high and the SI of AOT was low. The forest pixel has low reflectance in the VIS region ($0.45-0.69$); therefore, the effect of wv at the absorption features 0.58 and 0.65 μm was weak compared to the bare soil wv sensitivity indices. The forest and water pixels sensitivity indices are, therefore, similar in the VIS region. At bands with moderate absorption features, 0.72 and 0.82 μm, the dark target radiance is dominated by the scattering effect and the effect of wv is low. For the bright target, however, at these wavelengths, the scattering and absorption effects are nearly equal. This implies that at these wavelengths for bright target, both the scattering and absorption effects are important. From these results, we conclude that the influence of AOT on the reflectance in the spectral range ($0.44-0.96$) μm also depends on the surface albedo.

Case 2. Here, we only discuss those results which are relevant for the comparison between Cases 1 and 2. From the indices shown in Fig. 5(d)–(f), we observed that for Case 1, the sensitivity indices of AOT in the spectral range $0.44-0.96$ μm are high (>0.9). The AOT indices, however, vary at the water absorption features (0.58, 0.65, 0.72, 0.82, and 0.94 μm). This variation, however, is lower than in Case 1. Even at the principal absorption feature, SI indices for wv remain lower than AOT SI for all the surface albedo as in Case 1. Like, Case 1, the effect of surface types is noticeable. The reason for the difference in SI for the surface types has already been discussed for Case 1.

In both cases, the objective was to quantify the importance of the wv and AOT. We, however, observed that when the joint distribution was built using the probability densities and the relation between wv and $visibility$ (Case 2), the importance of the parameters, measured in terms of SI, is influenced by AOT. The primary cause of this influence is high variability in $visibility$ values. To measure the variability of wv and $visibility$, we used the coefficient of variation (CV). The CV represents the ratio of the standard deviation to the mean. The CV is a useful statistic to measure the relative variability for comparing different data series. From the image-based methods, in total, 1420 observations of $visibility$ were obtained; however, wv was observed at each pixel (7.87×10^5). The CV of wv and $visibility$ was 4.83% and 50.07%, respectively. The CV of the two parameters indicates that variability in $visibility$ values is larger than wv. There can be two reasons for the large variability in $visibility$ measurements. First, compared to wv, $visibility$ was observed at lower number of pixels. Second, the performance of the $visibility$ estimation method is influenced by the viewing and illumination geometry, and spatial heterogeneity. This happens because the image-based method is based on dense dark vegetation (DDV) technique and uses radiance values of pixels in red and NIR bands to search for the dense dark vegetation pixels.

To summarize, in this section, we have presented and discussed the sensitivity of the two atmospheric condition parameters as a function of wavelength, strength of the absorption feature, parameters uncertainty, and surface albedo. In Section II, we indicated that for a comparison purpose, we also quantified total sensitivity indices (TSIs) using the e-FAST method. The TSI is considered as a better estimation of sensitivity of parameters. However, on the basis of the results obtained from the e-FAST method, we observed that the difference between the two methods, as measured from their respective indices, were minor (<0.05). A possible explanation is that the sensitivity of the condition parameters is captured by the first-order Fourier coefficients; thus, the higher order terms that are calculated to quantify TSI do not carry much information about sensitivity to the parameters. This is because only two parameters were used in this study. For more parameters, the effect of higher order indices might be more useful. In [26], describing

the e-FAST method, the dependence of the interaction terms (higher order) to the number of factors is mentioned. The larger the number of factors, the higher the likelihood of substantial higher order terms. We have, therefore, not reported the results from the e-FAST method in this paper.

IV. Conclusion

In this paper, we have presented a methodology to quantify sensitivity of the estimated surface reflectance to water vapor concentration (wv) and AOT in the AC process. Besides quantifying the sensitivity indices, we also focused to analyze the effect of parameter's uncertainty, wavelength and surface albedo on these indices. Our approach was based on the FAST method that was implemented in an MCS framework. The methodology was applied to a hyperspectral image (HyMap) of the Millingerwaard area, The Netherlands. The AC was performed with the Central Data Processing Center (CDPC), which is an airborne processing chain at the Flemish Institute for the Technological Research (VITO).

The results of the SA, expressed as sensitivity indices, were presented for three surface albedo in the spectral range $0.44 - 0.96$ μm. The sensitivity of the estimate reflectance to wv and AOT depends on the wavelength, strength of the water absorption feature, parameters uncertainty, and on surface albedo.

1) Surface albedo: For the dark target, the estimated reflectance was more sensitive to AOT compared with wv over the $0.44-0.96$-μm spectral range with exception of the bands near the 0.94 water absorption feature, where the effect of wv and AOT is almost similar.
2) Strength of the absorption feature: For the bright targets, the sensitivity of the estimated reflectance to wv increases with the strength of the water absorption feature. For a dark target, however, except for the principal absorption feature near band 0.94 nm, the wv indices did not increase much compared to indices for bright targets.
3) Parameter uncertainty: If one parameter is more uncertain than the other, the SI is influenced by the more uncertain parameter. For instance, AOT's uncertainty was higher than wv's.

Therefore, AOT is an important parameter for dark targets for AC, more important than wv even at the principal absorption feature. For bright targets, the importance of wv and AOT depends on the strength of the absorption feature. AOT sensitivity indices were high for the nonabsorption water bands. We conclude that at the nonabsorption water bands AOT is a more important parameter compared to wv.

As an outlook from the study, we recommend to include the impact of uncertainty in the aerosol type in the SA. Like wv and AOT, knowledge about the type of atmospheric aerosol at the time of imaging is challenging to obtain. Often, expert judgment is used to select the appropriate aerosol type for the AC process. Therefore, it would be interesting to quantify the effect of the choice about the aerosol type on the estimated reflectance. Also, it might be more interesting to collectively study the impact of uncertainty in aerosol type, AOT, and wv by simultaneously varying them.

References

[1] C. Bohren and D. Huffman, *Absorption and Scattering of Light by Small Particles*. Hoboken, NJ, USA: Wiley, 2004.

[2] D. Burazerovic, R. Heylen, B. Geens, S. Sterckx, and P. Scheunders, "Detecting the adjacency effect in hyperspectral imagery with spectral unmixing techniques," *IEEE J. Sel. Topics Appl. Earth Observ. Remote Sens.*, vol. 6, no. 3, pp. 1070–1078, Jun. 2013.

[3] S. Chandrasekhar, *Radiative Transfer*. New York, NY, USA: Dover Publication Inc., 1960.

[4] J. Haan and J. Kokke, "Remote sensing algorithm development Toolkit I: Operationalization of atmospheric correction methods for tidal and inland waters," Netherlands Remote Sensing Board, Standard Guidelines NRSP-2 96–16, 1996.

[5] R. Richter, D. Schlapfer, and A. Muller, "An automatic atmospheric correction algorithm for visible/ NIR imagery," *Int. J. Remote Sens.*, vol. 27, no. 10, pp. 2077–2085, May 2006.

[6] A. Rodger and M. Lynch, "Determining Atmospheric Column Water Vapour in the 0.4–2.5 m spectral region," in *Proc. AVIRIS Workshop*, Pasadena, CA, USA, 2001.

[7] D. van de Vlag and A. Stein, "Incorporating uncertainty via hierarchical classification using fuzzy decision trees," *IEEE Trans. Geosci. Remote Sens.*, vol. 45, no. 1, pp. 237–245, Jan. 2007.

[8] M. S. Salama and A. Stein, "Error decomposition and estimation of inherent optical properties," *Int. J. Remote Sens.*, vol. 48, no. 26, pp. 4947–4962, 2009.

[9] J. Beekhuizen, G. Heuvelink, J. Biesemans, and I. Reusen, "Effect of DEM uncertainty on the positional accuracy of airborne imagery," *IEEE Trans. Geosci. Remote Sens.*, vol. 49, no. 5, pp. 1567–1577, May 2011.

[10] C. Liu, "Error propagation in atmospheric correction due to azimuthal angle simplification of lookup tables," *Int. J. Remote Sens.*, vol. 30, no. 2, pp. 275–282, 2010.

[11] D. Kaskaoutis, H. Kambezidis, A. Adamopoulos, and P. Kassomenos, "On the characterization of aerosols using the Angstrom, exponent in the athens area," *J. Atmos. Sol. Terr. Phys.*, vol. 68, no. 18, pp. 2147–2163, 2006.

[12] F. Seidel, A. Kokhanovsky, and M. Schaepman, "Fast retrieval of aerosol optical depth and its sensitivity to surface albedo using remote sensing data," *Atmos. Res.*, vol. 116, pp. 22–32, 2012.

[13] L. Guanter, L. Gómez-Chova, and J. Moreno, "Coupled retrieval of aerosol optical thickness, columnar water vapor and surface reflectance maps from envisat/meris data over land," *Remote Sens. Environ.*, vol. 112, no. 6, pp. 2898–2913, 2008.

[14] A. Saltelli, K. Chan, and E. Scott, *Sensitivity Analysis*. Hoboken, NJ, USA: Wiley, 2008.

[15] J. Biesemans *et al.*, "Image processing workflows for airborne remote sensing," in *Proc. 5th EARSeL Workshop Imaging Spectroscopy*, Bruges, Belgium, Apr. 2007 [Online]. Available: http://dev.eufar.net/document/publi/Biesemans_Earsel2007Bruges_20100421104411.pdf

[16] A. Saltelli, T. Andres, and T. Homma, "Sensitivity analysis of model output an investigation of new techniques," *Comput. Stat. Data Anal.*, vol. 15, pp. 211–238, 1993.

[17] A. Saltelli and J. Marivoet, "Non-parametric statistics in sensitivity analysis for model output: A comparison of selected techniques," *Reliab. Eng. Syst. Saf.*, vol. 28, pp. 229–253, 1990.

[18] G. Archer, A. Saltelli, and I. Sobol, "Sensitivity measure, anova-like techniques and the use of bootstrap," *J. Stat. Comput. Simul.*, vol. 58, pp. 99–120, 1997.

[19] I. Sobol, "Sensitivity analysis for nonlinear mathematical models," *Math. Modell. Comput. Exp.*, vol. 1, pp. 407–414, 1993.

[20] R. Cukier, H. Levine, and K. Shuler, "Nonlinear sensitivity analysis of multiparameter model systems," *J. Comput. Phys.*, vol. 26, pp. 1–42, 1978.

[21] A. Berk *et al.*, "Modtran4 user's manual," Air Force Res. Lab., Hanscom AFB, MA, USA, Tech. Rep., 1999.

[22] R. Richter, "Atmospheric/topographic correction for airborne imagery," in *ATCOR-4 User Guide, Version 4.2*. DLR-German Aerospace Center, Remote Sensing Data Center, 2007 [Online]. Available: http://www.rese.ch/pdf/atcor4_manual.pdf

[23] E. Shettle and R. Fenn, "Models for the aerosols of the lower atmosphere and the effects of humidity variations on their optical properties," Air Force Geophys. Lab., USA, Tech. Rep. AFGL-TR-79-0214 Environmental Research Papers No. 676, 1979.

[24] G. d'Almeida, P. Koepke, and E. Shettle, *Atmospheric Aerosols Global Climatology and Radiative Characteristics*. Hampton, VA, USA: A. Deepak Pub, 1991.

[25] G. McRay, W. Tilde, and J. Seinfeld, "Global sensitivity analysis—A computational implementation of the fourier amplitude sensitivity test (fast)," *Comput. Chem. Eng.*, vol. 6, no. 1, pp. 15–25, 1982.
[26] A. Saltelli, S. Tarantola, and K. Chan, "A quantitative model-independent method for global sensitivity analysis of model output," *Technometrics*, vol. 41, no. 1, pp. 39–56, 1999.
[27] W. Verhoef and H. Bach, "Simulation of hyperspectral and directional radiance images using coupled biophysical and atmospheric radiative transfer models," *Remote Sens. Environ.*, vol. 87, no. 1, pp. 23–41, 2003.
[28] S. M. Adler-Golden *et al.*, "Atmospheric correction for shortwave spectral imagery based on modtran4," in *Proc. SPIE*, 1999, vol. 3753, pp. 61–69.
[29] R. Lindstrot *et al.*, "1d-var retrieval of daytime total columnar water vapour from MERIS measurements," *Atmos. Meas. Techn.*, vol. 5, no. 3, pp. 631–646, 2012.

Nitin Bhatia received the Diploma degree in electrical engineering from the Aryabhat Polytechnic, Delhi, India, in 2003, the Engineering degree in computer science (IT) from Indraprastha University (GGIPU), Delhi, India in 2006, the M.Sc. degree in geoinformatics from the University of Twente (ITC), Enschede,The Netherlands, in collaboration with Indian Institute of Remote Sensing (ISRO), Dehradun, India, in 2010. He is currently pursuing the Ph.D. degree in earth observation from ITC.

His research interests include uncertainty and SA of remote sensing products developed in remote sensing processing chain, AC, and statistical analysis of remotely sensed images.

Valentyn A. Tolpekin received the M.Sc. degree in theoretical physics from Odessa State University, Odessa, Ukraine, in 1997, the M.Sc. degree in computer science from South Ukrainian Pedagogical University, Odessa, Ukraine, in 1998, and the Ph.D. degree in physics from the University of Twente (ITC), Enschede, The Netherlands, in 2004. Currently, he is an Assistant Professor with the Department of Earth Observation Science, Faculty of Geo-Information Science and Earth Observation, ITC. His research interests include statistical analysis of remotely sensed images, optical, and radar.

Ils Reusen received the M.Sc. degree in physics (astronomy) and the Ph.D. degree in physics (nuclear astrophysics and spectroscopy) from Katholieke Universiteit Leuven (KU Leuven), Leuven, Belgium, in 1993 and 1999, respectively.

After her Ph.D. degree, she had a 6-month Postdoctoral position in image processing with the Electrical Engineering Department, KU Leuven. After that, she joined the Research Unit Remote Sensing and Earth Observation Processes, Flemish Institute for Technological Research (VITO), Mol, Belgium. She has been active in airborne hyperspectral remote sensing since 2000. Her research interests include the radiometric calibration of the future PROBA-V Earth Observation sensor using ground-based hyperspectral reflectance measurements and APEX under flights.

Dr. Reusen is a member of the scientific committees of EARSeL SIG Imaging Spectroscopy, WESSEX Forest Fires, and Whispers. She is a member of the ISPRS Technical Commission I Working Group 1 of Airborne Platform Interface." In 2007, she chaired the International 5th EARSeL SIG Imaging Spectroscopy Workshop.

Sindy Sterckx received the M.Sc. degree in bio-engineering from Katholieke Universiteit Leuven, Leuven, Belgium, in 1999.

After working as a Research Associate with Katholieke Universiteit Leuven for 2 years, she joined the Research Unit Remote Sensing and Earth Observation Processes, Flemish Institute for Technological Research (VITO), Mol, Belgium, in 2001. Currently, she is responsible for the Image Quality Center of ESAs Proba-V satellite mission, where she is in charge of the in-flight radiometric calibration activities. Her research interests include AC, adjacency correction, water quality, and vicarious calibration.

Jan Biesemans received the M.Sc. and Ph.D. degrees in agricultural and applied biological sciences (soil physics and hydrology) from Ghent University, Ghent, Belgium, in 1995 and 2000, respectively.

After 5 years of academic research and teaching activities, he worked for about 2 years as a C++ Software Development Engineer in the prepress industry. After this period, he worked for 2 years as an Independent Consultant for private, governmental, and intergovernmental organizations, focused on the generation of custom-made software solutions for specific data analysis problems in the field of spatial epidemiology and modelling of environmental processes. In June 2004, he then became a Project Coordinator with the Flemish Institute for Technological Research (VITO), Mol, Belgium, where he currently coordinates in software development activities with respect to unmanned aerial vehicle ground segments and specific airborne imaging projects.

Alfred Stein is a Professor of Spatial Statistics and Image Analysis with the Faculty of Geo-Information Science and Earth Observation (ITC), University of Twente, Enschede, The Netherlands. His research interests focus on the statistical aspects of spatial and spatiotemporal data.

Prof. Stein became the Editor-in-Chief of *Spatial Statistics*, which is now the leading platform in the field of spatial statistics, in 2012. Since 2008, he is a member of the Management Team of the Faculty. He is a member of the Socio-Economic and Natural Sciences of the Environment (SENSE) Research School.